Bull Volcanol (2010) 72:469–485
DOI 10.1007/s00445-009-0331-5

RESEARCH ARTICLE

Explosive lava–water interactions II: self-organization processes among volcanic rootless eruption sites in the 1783–1784 Laki lava flow, Iceland

Christopher W. Hamilton · Sarah A. Fagents · Thorvaldur Thordarson

Received: 22 May 2009 / Accepted: 1 December 2009 / Published online: 3 February 2010

Abstract We have applied quantitative geospatial analyses to rootless eruption sites in the Hnúta and Hrossatungur groups of the 1783–1784 Laki lava flow to establish how patterns of spatial distribution can be used to obtain information about rootless cone emplacement processes and paleo-environments. This study utilizes sample-size-dependent nearest neighbor (NN) statistics and Voronoi tessellations to quantify the spatial distribution of rootless eruption sites and validate the use of statistical NN analysis as a remote sensing tool. Our results show that rootless eruption sites cluster in environments with abundant lava and water resources, but competition for limited groundwater in these clusters can cause rootless eruption sites to develop repelled distributions. This pattern of self-organization can be interpreted within the context of resource availability and depletion. Topography tends to concentrate lava (fuel) and water (coolant) within topographic lows, thereby promoting explosive lava–water interactions in these regions. Given an excess supply of lava within broad sheet lobes, rootless eruption sites withdraw groundwater from their surroundings until there is insufficient water to maintain analogs to explosive molten fuel–coolant interactions. Rootless eruption sites may be modeled as a network of water extraction wells that draw down the water table in their vicinity. Rootless eruptions at locations with insufficient groundwater may either fail to initiate or terminate before explosive activity has ceased at nearby locations with a greater supply of water, thus imparting a repelled distribution to observed rootless eruption sites.

Keywords Volcanic rootless cones · Pseudocraters · Phreatomagmatic · Explosive lava–water interactions · Laki · Iceland · Mars

Editorial responsibility: J. White

Electronic supplementary material The online version of this article (doi:10.1007/s00445-009-0331-5) contains supplementary material, which is available to authorized users.

C. W. Hamilton (✉) · S. A. Fagents
Hawai'i Institute of Geophysics and Planetology,
University of Hawai'i,
1680 East-West Road,
Honolulu, HI 96822, USA
e-mail: christopher@higp.hawaii.edu

T. Thordarson
School of Geosciences, University of Edinburgh,
Edinburgh, Scotland, UK

Introduction

Volcanic rootless cones, also known as pseudocraters, are generated by explosive lava–water interactions (Thorarinsson 1951, 1953). Rootless cone groups on Earth typically include tens to thousands of explosion sites, with individual cones ranging 1–35 m in height and 2–450 m in basal diameter (Fagents and Thordarson 2007). Terrestrial rootless cones and analogous structures on Mars are observable in remotely sensed imagery (e.g., Allen 1979; Frey et al. 1979; Frey and Jarosewich 1982; Lanagan et al. 2001; Greeley and Fagents 2001; Fagents et al. 2002; Head and Wilson 2002; Bruno et al. 2004, 2006; Baloga et al. 2007; Fagents and Thordarson 2007; Jaeger et al. 2007, 2008a). With the exceptions of Bruno et al. (2004, 2006) and Baloga et al. (2007), previous studies have focused on the morphological characteristics of rootless cones rather than exploring their patterns of spatial organization. In this study, we build on the morphological investigations of Hamilton et al. (2010) to explore how the spatial distribution of rootless eruption sites can be used to infer the availability of water and lava at different scales, constrain underlying physical process, and establish non-

morphological criteria for identifying volcanic rootless cones on Mars.

Background information

Geological setting of the study region

The Laki eruption initiated in southern Iceland (Fig. 1) on June 8, 1783 and continued until February 7, 1784 (Thordarson 2003a, 2003b). During 8 months of activity, ten *en echelon* fissures propagated northwest to produce a 27 km-long cone row with associated lava flows covering 599 km^2 (Thordarson and Self 1993). The dense rock equivalent volume of the erupted tholeiitic magma was 15.1 ± 1 km^3, of which 97.4% was emplaced as lava flows (Thordarson et al. 1996). Lava was channeled from the Síða highlands to the coastal lowlands through the Skaftá and Hverfisfljót River gorges (Thordarson and Self 1993). Lava entering the Skaftá River gorge flowed from the Laki cone row through the valleys of Úlfarsdalur and Varmárdalur (Steingrimsson 1788; Thordarson and Self 1993; Thordarson 2003a, b).

This study focuses on rootless cones located in the southern region of Varmárdalur, near the axis of the Galti-Hrossatungur ridge, which lies ~3–5 km south–southeast of Laki fissures 1 and 2 (Hamilton et al. 2010). The study area covers a total area of 2.77 km^2 (Fig. 1) and includes two main rootless cone groups: Hnúta and Hrossatungur. Hamilton et al. (2010) determined that the Hnúta and Hrossatungur groups are composite landforms that include six constituent domains (Fig. 1a). Domain 1 of the Hnúta group was the first to form and includes a large (390,224 m^2) platform-shaped rootless tephra complex and a series of smaller (504 to 31,649 m^2) complexes that extend northeast—we refer to the largest of these satellite complexes as subdomain 1.1 ("S1.1" in Fig. 1b). Domain 2 overlies the southern margin of domain 1 and the adjacent terrain. The Hrossatungur group is located farther to the south and covers 153,658 m^2. Hamilton et al. (2010) used superposition relationships and tephrostratigraphy to define four domains within the Hrossatungur group. Within each of these domains, we isolate subdomains with >30 rootless eruption sites—all of which exhibit strong evidence for contemporaneous formation within a continuous geographic region. These subdomains are labeled "S3.1," "S4.1," "S5.1," and "S6.1" in Fig. 1b.

Previous studies of geospatial distribution

Bruno et al. (2004) investigated the nearest neighbor (NN) statistics of rootless cones in the Hnúta group using digitized crater centers based on 1:37,000 grayscale aerial photographs.

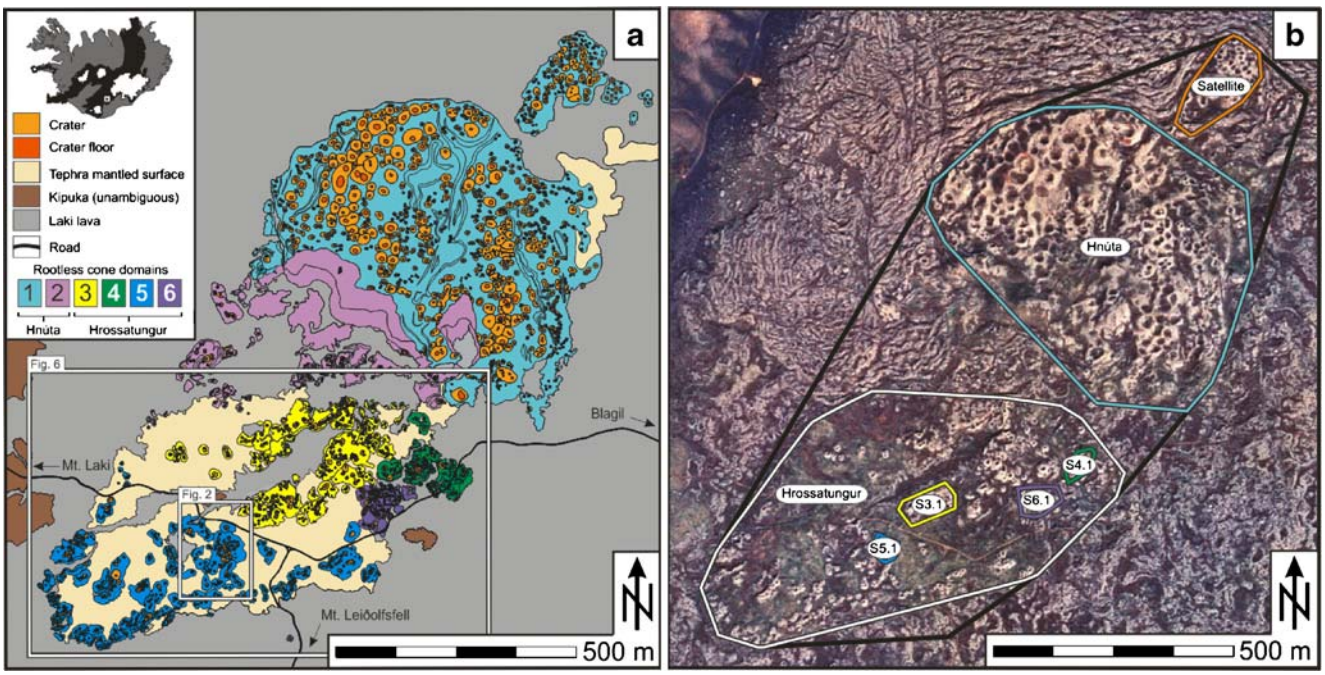

Fig. 1 The study area is located within the 1783–1784 Laki lava flow which originates from a fissure system in the active volcanic zone (*black*) of Iceland (*inset*). **a** Rootless tephra deposits in the Hnúta and Hrossatungur groups divided into six independently formed domains based on contact relationships and tephrochronology (Hamilton et al. 2010). **b** We examine the spatial statistics of rootless eruption sites within eight regions: (1) complete study area (bounded by a *black* convex hull); (2) Hnúta group (*turquoise*); (3) Hnúta satellite subdomain 1.1 (*orange*), and (4) Hrossatungur group (*white*), which includes four subdomains, (5) S3.1 (*yellow*); (6) S4.1 (*green*); (7) S5.1 (*cyan*); and (8) S6.1 (*purple*)

They determined that the area of the Hnúta group is ~1 km^2 and that it includes 660 explosion sites. To determine the area of their input distributions, Bruno et al. (2004) rotated their images through 1° increments to find the minimum rectangular area that enclosed the complete group of features. The resulting NN statistics (R=0.68 and c=15.54; see Table 1 and "Review of nearest neighbor analysis methods" for definitions of R and c) led Bruno et al. (2004) to conclude that the Hnúta group exhibits a non-random spatial distribution with NN distances being less than expected by a Poisson model due to systematic controls exerted by the geometry of underlying lava pathways and/or substrate hydrology.

Bruno et al. (2006) reexamined the NN distribution of the Hnúta group using an improved methodology that employs a convex hull to define study area boundaries. Bruno et al. (2006) divided the Hnúta group into north and south subgroups, which correspond to our Hnúta and Hrossatungur groups, respectively. They identified 357 explosion sites (including 344 interior sites, N_i; see Table 1 and "Review of nearest neighbor analysis methods" for definitions of notation) in Hnúta north and 301 (N_i=289) explosion sites in Hnúta south. The explosion sites were defined by digitizing the centers of craters using 1:37,000 grayscale aerial photographs. Examination of NN distances between rootless eruption sites in Hnúta north showed that R=0.83 and c=−6.15, whereas in Hnúta south, R=0.74 and c=−8.52. These results confirmed that the Hnúta rootless eruption sites exhibit statistically significant non-random distributions (at the 2σ confidence level), and both the north and south populations are clustered relative to the Poisson model. Bruno et al. (2006) also introduced skewness and kurtosis measures to distinguish between landforms with otherwise similar NN statistics (e.g., volcanic rootless cones, secondary impact craters, and ice-cored mounds such as pingos).

Given the limited resolution of their input data, Bruno et al. (2004, 2006) were able to discern only 30% of the rootless explosion sites identified in the same area by Hamilton et al. (2010). Bruno et al. (2004, 2006) also lacked the field observations required to identify rootless cone domains, delimit domain boundaries, and constrain their emplacement chronology. To show the effects of scale on rootless cone emplacement processes and their resulting patterns of geospatial organization, we reexamine the spatial distribution of rootless explosion sites in the Hnúta and Hrossatungur groups using higher resolution inputs obtained from differential global positioning system (DGPS) surveys and an improved NN methodology that accounts for sample-size-dependent biases in NN statistics (Baloga et al. 2007; Beggan and Hamilton 2009).

Methods

Geological mapping

To examine the spatial distribution of rootless eruption sites within the Hnúta and Hrossatungur groups, we constructed

Table 1 Statistical nomenclature

Variable	Definition
A	Area of a feature field
A_{hull}	Area of the convex hull
c	Statistic for comparing actual (r_a) to expected (r_e) mean NN distances, $c=(r_a/r_e)/\sigma_e$
k	Poisson index
N	Number of features within a sample population
N_i	Number of features within the convex hull
N_v	Number of features forming the vertices of the convex hull
P	Probability
R	Statistic for comparing actual (r_a) to expected (r_e) mean NN distances, $R=r_a/r_e$
r	Radial distance
r_a	Mean NN distance observed in the data
r_e	Mean NN distance calculated from a given NN model (e.g., Poisson)
$P(r)$	Population density function describing the expected radial distance between objects
ρ_0	Population (spatial) density of the input features, $\rho_0=N/A$
ρ_i	Population (spatial) density of the input features, $\rho_i=N_i/A_{hull}$
σ	Standard deviation
σ_e	Standard error, $\sigma_e=\sigma/\sqrt{N}$ and for a Poisson NN distributions $\sigma_e=0.26136/\sqrt{N\rho_0}$
V	Statistic for comparing actual (v_a) to expected (v_e) mean Voronoi cell areas, $V=v_a/v_e$
v_a	Mean Voronoi cell area observed in the data
v_e	Mean Voronoi cell area for a hexagonal distribution with NN distances = r_a

digital facies maps of the study area using field observations, DGPS surveys, interpretations of color aerial photographs (0.5 m/pixel), and geographic information systems (GIS). We used DGPS to delimit the morphological facies of rootless cones throughout the complete study area and develop a 0.19 m/pixel digital terrain model (DTM) for a 57,630 m^2 (212.5×271.2 m) region within domain 5 of the Hrossatungur group. Appendix 1 of Hamilton et al. (2010) explains the DGPS data processing methodology. This DTM region was chosen because it includes excellent examples of the three basic rootless cone archetypes: (1) tube-fed, (2) channel-fed, and (3) broad sheet lobe-fed (Hamilton et al. 2010). The third rootless archetype is of particular significance because broad flows can more easily host simultaneously active eruption sites with independent access to lava. This allows us to test the hypothesis that in the presence of excess lava, rootless eruption sites will compete for limited water resources and develop a spatial arrangement that maximizes the utilization of available groundwater.

Review of nearest neighbor analysis methods

The NN method was developed by Clark and Evans (1954) to quantify the spatial distribution of objects that can be approximated as points. Euclidean distances are calculated between each point and the other members of the distribution to identify the distance between all NN pairs. The mean NN distance (r_a) in the input distribution is compared to the mean NN distance that would be expected (r_e) if the features were distributed according to some theoretical model. The ratio of the observed-to-expected separation, R, is given by:

$$R = \frac{r_a}{r_e}. \quad (1)$$

If $R \approx 1$, then the observed spatial distribution fits the model. If $R<1$, then object separations are closer than predicted, which implies that an underlying process is drawing the objects together into clusters. Alternatively, if $R>1$, then objects are more widely spaced than predicted, which implies that interactions between objects have caused them to repel. The significance of R is assessed using a test statistic (c), which is defined as:

$$c = \frac{r_a - r_e}{\sigma_e} \quad (2)$$

where σ_e is the standard error of the mean NN distance in the expected distribution (Table 1). To test for spatial randomness, Clark and Evans (1954) chose to use the following Poisson probability density function, $\rho(r)$, for calculating expected NN locations:

$$\rho(r) = \frac{dP}{dr} = 2\pi\rho_0 e^{-\rho_0 \pi r^2} \quad (3)$$

where P is the probability, r is radial distance, and ρ_0 is spatial density, which is calculated by dividing the number of objects (N) by the area of the feature field (A).

Baloga et al. (2007) recognized that Poisson NN distances assume an infinite domain and azimuthal symmetry about any arbitrarily chosen point. Finite boundaries could pose a limitation; however, they conclude that in most practical situations, the exponential decay in Eq. 3 limits the maximum NN distance to finite values, and edge effects are generally minor because the boundary of the region increases with r while the area of the region increases by r^2. Bruno et al. (2006) applied the convex hull solution to determine boundaries for their input data and minimize edge effects. The convex hull is a polygon defined by the outermost points in a feature field such that each interior angle of the polygon measures less than 180º (Graham 1972). To ensure that every point has a valid NN within the area of the convex hull (A_{hull}), each point inside the convex hull is allowed to search for a NN among the interior points, N_i, and those located at the vertices of the convex hull, N_v. However, N_v are not permitted to search for NNs because their closest neighbor may be located outside of the study region. The interior population density ($\rho_i = N_i/A_{hull}$) thus substitutes for ρ_0 in Eq. 3 and provides an estimate of the true density within an infinite domain.

Frequency distributions of NN distances generated by a random process should match the Poisson probability density distribution, but this is rarely the case due to sampling variations. For instance, in a Poisson random distribution of points, R should ideally equal 1, and c should equal 0±1.96 and 0±2.58, at the 0.95 and 0.99 confidence levels, respectively (Clark and Evans 1954), but these values implicitly assume large sample sets ($N>10^4$ features). For smaller populations, Baloga et al. (2007) determined that R and c are greater than predicted by classical NN theory. In addition to developing sample-size-dependent tests for Poisson randomness, Baloga et al. (2007) proposed three novel NN models:

1. *Normalized Poisson NN distributions* account for minimum feature size and/or resolvable NN distance in the dataset by modifying r_e, σ_e, skewness, and kurtosis based on a user-defined distance threshold.
2. *Scavenged Poisson NN distributions* assume features consume (scavenge) resources in their surroundings, which affects the kth nearest neighbor by increasing r_e relative to the standard Poisson NN model. The Poisson index, k, specifies the number of neighboring features that participate in the scavenging process, and if $k=0$, the standard Poisson NN model is obtained.

3. *Logistic NN distributions* apply the classical probability distribution for self-limiting population growth due to the use of available resources, thus making the NN distribution more uniform and leading to smaller skewness, but larger kurtosis values relative to the Poisson NN model.

Geospatial analyses: methodology

To investigate the spatial organization of volcanic rootless cones, Hamilton et al. (2007) wrote a MATLAB program that automates Poisson NN analyses using the convex hull solution for defining input data boundaries (Bruno et al. 2006) and sample-size-dependent calculations of R and c (Baloga et al. 2007). Beggan and Hamilton (2009) developed this MATLAB program into the "nearest neighbor analysis" module of their Geological Image Analysis Software (GIAS; www.geoanalysis.org). GIAS tests for four NN distributions: (1) Poisson, (2) normalized Poisson, (3) scavenged, k=1, and (4) scavenged, k=2. Beggan and Hamilton (2009) provide detailed descriptions of the "nearest neighbor analysis" module, derivation of the k=2 case for scavenged Poisson distributions, and calculations of sample size thresholds required to discriminate between the standard Poisson and scavenging k=1 and 2 cases. For reasons discussed below, we focus on the Poisson NN distribution model in this study.

In most geological applications, there are NNs below a threshold distance that cannot be resolved due to resolution limitations of the data and/or masking of features by later processes (Baloga et al. 2007). In such instances, it is necessary to apply a normalization technique. Pixel dimensions can be used to estimate the detection limit of landforms in remote sensing imagery, but in this study, the location of rootless eruption sites were calculated as the centroids of rootless crater floors that were delimited using field-based DGPS measurements. In the field, the smallest rootless crater floor that we identified was 0.21 m in diameter, which is above the precision of our DGPS surveys (~0.06 m for replicated DGPS transects). Normalization is therefore not required to correct for limitations in the resolution of our input data. Nevertheless, the use of high spatial resolution data does not exclude the possibility that overprinting may have affected the observed NN distributions. For instance, the surface expression of rootless eruption sites could have been obscured by a variety of mechanisms, including subsequent rootless explosions, tephra deposition, erosion, and/or sedimentary mantling. In some cases, overprinting processes may have contributed to the development of repelled NN distributions by obscuring rootless eruption sites that became inactive before explosive activity had ceased at neighboring localities ("Scale-dependent controls on the spatial distribution of rootless eruption sites"). Overprinting may therefore affect the preservation of rootless eruption sites, but the overprinting process cannot be described by a constant length scale because it involves multiple mechanisms that could each operate over a range of scales (e.g., overprinting by rootless tephra deposition may vary with eruption duration and intensity and thus cannot be regarded as a uniform process). Since our dataset is not limited by input data resolution and overprinting processes in our study area are non-uniform, we conclude that the use of a constant normalization term would not provide meaningful results, and thus, we omit further discussion of the normalized Poisson model.

Discrimination between Poisson NN (k=0) and scavenged Poisson NN (k>0) distributions depends upon the minimum number of objects, population density, and the order (k) of the scavenging model. Beggan and Hamilton (2009) calculated that for population densities of 0.0005–0.5 objects/unit area, and a confidence level of 0.95, at least 50 to 60 objects are required to distinguish between Poisson and k=1 scavenged Poisson distributions, whereas at least 100 to 150 objects are required to distinguish between k=1 and 2 distributions. Except for subdomain 5.1, all of the input distributions in our study contain a sufficient number of objects to confidently discriminate between k=0 and k=1 NN distributions. For each of these regions, k=1 scavenging models consistently overestimate r_e relative to r_a, with c being outside the 2σ confidence limits and R exceeding the lower 2σ threshold (Appendix 1). Consequently, the k=1 model fails to accurately describe any of the input NN distributions. For higher order NN analyses, only three of the eight input distributions have enough objects to distinguish between the k=1 and 2 models. Given that expected NN distances (r_e) increase as the order of k increases and all of the input distributions exhibit clustering relative to the k=1 model, it would be impossible for the k=2 model to provide a statistically significant fit for any of the input distributions.

To obtain input coordinates for our NN analyses, we used ArcGIS to calculate the centroids for every rootless crater floor polygon in the geospatial database—under the assumption that the crater floor centroids best approximate the distribution of the underlying rootless eruption sites. We parsed the centroids into eight geographic subsets (Fig. 1b), which include: (1) all of the rootless eruption sites in the Hnúta and Hrossatungur groups; (2) domain 1 of the Hnúta group (excluding the satellite complexes to the northwest); (3) subdomain 1.1 of the Hnúta group (consisting of the largest satellite rootless tephra complexes); (4) the Hrossatungur group as a whole (including domains 3–6); and (5–8) the four subdomains within the Hrossatungur group. We did not analyze the spatial distribution of explosion sites within domain 2 of the Hnúta group because rootless tephra deposits have been poorly preserved due to widespread lava rafting and inundation.

We also used Voronoi tessellations to examine the spatial characteristics of the rootless eruption sites. Voronoi tessellation, also known as Thiessen or Dirichlet tessella-

tion, divides a region into a set of polygons, the boundaries of which are perpendicular bisectors of the lines joining NN points. Voronoi cells thus represent the regions over which each object exerts the greatest influence. To maximize the utilization of homogeneously distributed resources, each member of a group must develop a maximal spacing from its neighbors, thus generating a Voronoi tessellation with cells of equal area. This arrangement would occur within a uniform spatial distribution in which R would achieve its theoretical maximum value of 2.1491 (Clark and Evans 1954). We derived the following equation from basic geometric principles to calculate the optimum Voronoi cell area (v_e) that would be expected if we assume a maximum packing arrangement with all NN distances equal to r_a, which would produce a tessellation of equally sized hexagonal cells:

$$v_e = \frac{\sqrt{3}}{2} {r_a}^2. \quad (4)$$

We compare the mean Voronoi cell area (v_a) within each of the eight study regions to v_e. If rootless eruption sites tend toward an optimum configuration for utilizing available resources, then the ratio of v_a to v_e, which we call V, will approach 1. To prevent degenerate solutions (e.g., unbounded cells of infinite area), we remove Voronoi cells that extend beyond the convex hull of each input distribution.

Results

Digital terrain model and stratigraphy

We discuss the geology of the DTM region (Fig. 2) to demonstrate the general characteristics of rootless cones and document the criteria used for selecting the subdomains examined in our geospatial analyses. The DTM includes examples of three archetypical rootless cone types: (1) tube-fed; (2) channel-fed; and (3) broad sheet lobe-fed. Representative examples of each of these archetypes are identified by in the DTM presented in Fig. 2a. The corresponding facies map (Fig. 2b) depicts lava exposures, inferred lava flow directions, morphological subdivisions within the rootless cones, rootless eruption site locations,

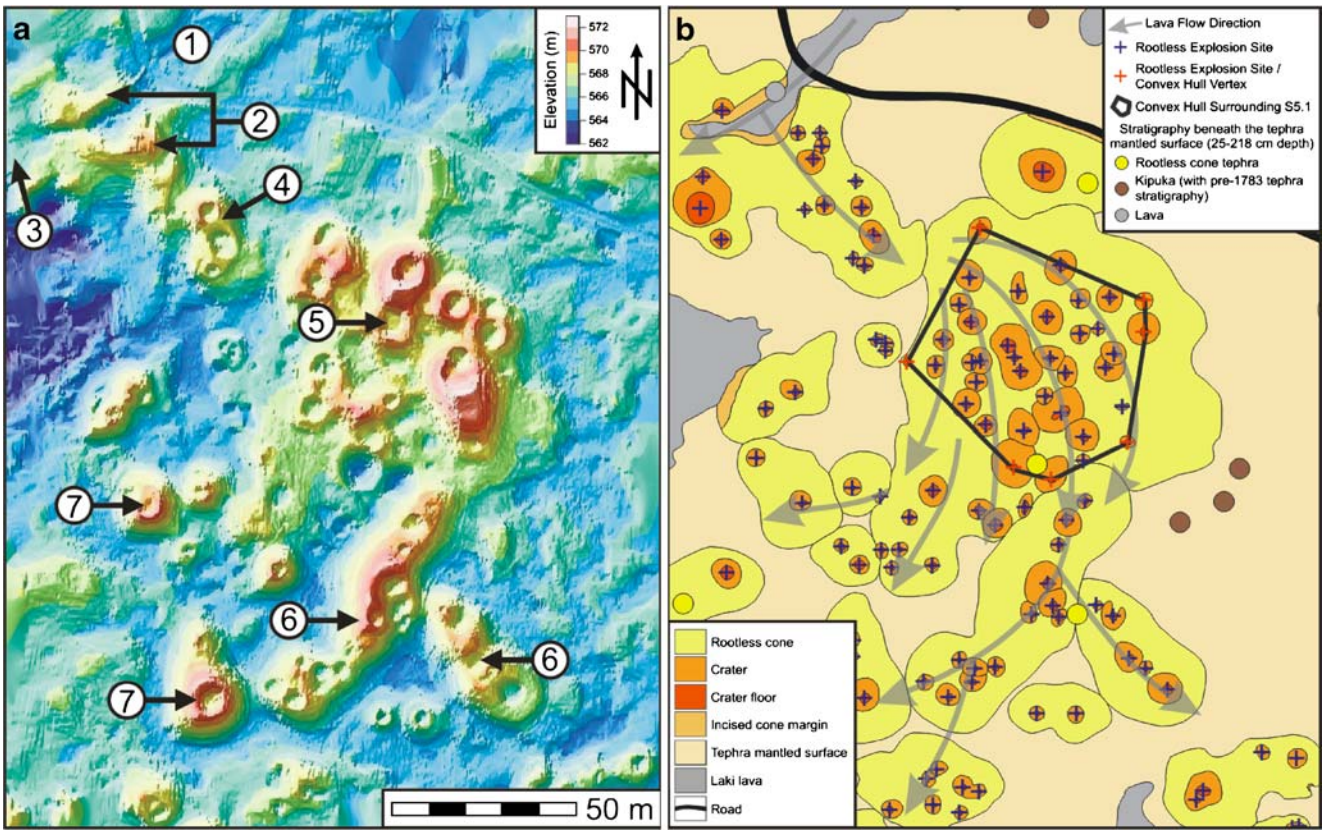

Fig. 2 **a** Digital terrain model (*DTM*) in plan view showing a southwest flowing lava channel ("1"), paired half-cone rootless tephra deposits ("2"), lava-rafted tephra accumulation ("3"), linearly aligned tube-fed rootless tephra deposits ("4" and "6"), sheet lobe-fed rootless eruption sites ("5"), and radially symmetric tube-fed rootless tephra deposits ("7"). **b** Corresponding ArcGIS map showing Subdomain 5.1 (bounded by the convex hull) with crater floor centroid locations (*crosses*). *Color codes* in the geological map follow the conventions of Hamilton et al. (2010)

the convex hull bounding subdomain 5.1, and the near-surface stratigraphy identified within nine excavation sites.

Lava entered the DTM region through a southwest flowing channel ("1" in Fig. 2a) that occupies a linear topographic depression bounded on either side by kipuka (i.e., surfaces that were not inundated by lava during the most recent episode of flow emplacement). These kipuka exhibit continuous soil sequences that include tephra layers ranging from the 1918 Katla eruption to the 870 Veiðivötn eruption (Hamilton et al. 2010). The absence of intervening lava flows within these continuous soil sequences, and their higher elevation relative to the surrounding lava demonstrate that the kipuka are remnants of paleotopographic highs that were not inundated by lava during the 1783–1784 Laki eruption. In Fig. 2b, excavation sites into kipuka with continuous soil sequences are identified by brown circles.

Throughout the Hnúta and Hrossatungur groups, Hamilton et al. (2010) examined the tephrostratigraphy within 81 excavation sites and determined that the Laki lava flow was confined by kipuka and must therefore have been concentrated into topographic lows that existed before June 8, 1783. Hamilton et al. (2010) suggested that prior to the Laki eruption, the DTM region (Fig. 2) included a series of water drainage channels that had incised into the southward dipping slope of the Galti-Hrossatungur ridge, but that these boggy paleotopographic depressions were inundated by lava as the Laki flow advanced southward toward Mt. Leiðólfsfell. Along the lava flow path, rootless eruptions typically inverted the landscape by constructing rootless tephra accumulations that exceeded the elevation of the pre-eruption topography. The spatial distribution of explosive lava–water interactions that formed the Hnúta and Hrossatungur groups must therefore be influenced by initial topography because rootless eruptions could not have been generated above paleotopographic highs that were not covered by lava.

Channel-fed rootless eruptions in the northwest corner of Fig. 2 deposited tephra onto the surface of stationary lava levees and the adjacent kipuka. The resulting tephra deposits have a paired half-cone morphology ("2" in Fig. 2a) with two crescent-shaped segments separated by a trough aligned with the axis of the channel. The axial trough formed as channel-fed rootless eruptions generated radial distributions of tephra that were emplaced onto both stationary and actively flowing lava surfaces. Tephra landing on stationary surfaces on either side of the lava channel accumulated to form paired half-cone deposits, whereas tephra landing on the moving lava was transported away from the depocenter. Rafted tephra associated with this event generated a down-flow accumulation of material ("3" in Fig. 2a) that connects the two crescent-shaped segments on either side of the lava channel axis. The paired half-cone archetype and lava-rafted tephra deposits are analogous to the elongated rootless cones and associated tephra wakes that have been documented on Mars (Jaeger et al. 2007, 2008a). Jaeger et al. (2008b) predicted that these landforms should also be found in near-vent regions on Earth where voluminous lava flows advanced over wet or frozen ground. Prior to this study, elongate rootless tephra morphologies and tephra wakes had not been documented on Earth outside of littoral settings, but our observations confirm the prediction by Jaeger et al. (2008b).

The paired half-cone deposits in the DTM region ("2" in Fig. 2a) are situated at a junction between a southwest-flowing lava channel ("1" in Fig. 2a) and southeast-branching lava tube that fed a linear alignment of rootless eruption sites ("4" in Fig. 2a). The tube extends 50–55 m before widening into a broad sheet lobe, which is bounded to the east by a paleotopographic high—as evidenced by continuous soil sections that contain tephra layers predating the Laki eruption (identified by brown circles in Fig. 2b). The sheet lobe hosts numerous rootless eruption sites ("5" in Fig. 2a) and curves to the south along the kipuka margin before developing into a network of lava tubes with overlying rootless tephra deposits. Linearly aligned rootless eruption sites along some of the tube segments have produced interfingered and elongated rootless tephra deposits ("6" in Fig. 2a), whereas tube-fed rootless eruption sites that are more widely separated have generated tephra deposits with radial symmetry about a central crater ("7" in Fig. 2a).

The sheet lobe-fed rootless cones (bounded by the convex hull region in Fig. 2b) are of particular interest because they show evidence of contemporaneous emplacement and lack of linear alignment. The state of stress at the base of narrow lava pathways (e.g., tubes and channels) favors the formation of linearly aligned rootless cones (Hamilton et al. 2010), whereas sheet lobes have a more widely distributed lava supply and can thus support numerous rootless eruptions with independent access to lava. Given the spatter-rich nature of rootless tephra in subdomain 5.1 and the presence of lava mantling the interior walls of the up-flow paired half-cone deposits ("2" in Fig. 2a), we conclude that this region had an excess supply of lava and that groundwater was the limiting reagent during the rootless eruptions. Consequently, subdomain 5.1 provides an ideal test case for examining the effect of limited water resources on the spatial organization of contemporaneously active rootless eruption sites.

Geospatial analyses: results

NN analyses

Comparison of object locations relative to expected patterns of distribution allows for testing of spatial organization models. We compare the distribution of rootless eruption sites to a Poisson (random) model using two test statistics,

R (Eq. 1) and c (Eq. 2). Using sample-size-dependent values of R, c and their respective thresholds of significance, the following scenarios are possible. If R and c fall within $\pm 2\sigma$ of their expected values, then the spatial distribution is consistent with the model. If c is outside the range of $\pm 2\sigma$, then the inference is that the distribution is inconsistent with the model regardless of the value of R. If c is outside $\pm 2\sigma$ and R is greater than the $+2\sigma$ threshold, then the input distribution exhibits a statistically significant repelling relative to the model. Conversely, if c is outside the $\pm 2\sigma$ range and R is less then than the -2σ threshold, then the input distribution is inferred to be clustered relative to the model. If R is outside $\pm 2\sigma$ and c is within the $\pm 2\sigma$ range, then the test results are ambiguous, which generally indicates that there are insufficient data to perform the analysis and/or the standard error (σ_e) of the input distribution is large.

Table 2 and Fig. 3 summarize the measured properties of the eight input distributions. Table 3 and Figs. 4 and 5 summarize the results of the Poisson NN analyses. For the study area as a whole, the mean expected NN distance (r_e) is 12.05 m ($\sigma_e \pm 0.14$ m), which is 3.38 m larger than r_a. The resulting ratio of r_a to r_e (i.e., R) is 0.72, and the confidence measure (c) is −25.14. These R and c values are well outside their respective 2σ limits of significance, and thus, we reject the Poisson model as a description of the input NN distribution. However, given that R exceeds its lower sample-size-dependent limit (at 2σ), we infer that the rootless eruption sites within the complete study area exhibit a statistically significant clustering, relative to the Poisson model. This result agrees with our field observations which show that over large regions, rootless eruption sites concentrate within lava-inundated topographic lows to form clusters of high population density that are separated by kipuka with zero population density. Thus, when applying NN analyses, it is important to use geological information to delimit logical boundaries around features that share a common formation environment and time of emplacement.

Within our study area, we have used stratigraphy and tephrochronology to isolate two rootless cone groups (i.e., Hnúta and Hrossatungur) and a series of domains and subdomains. In the Hnúta group (domain 1), r_e is 11.92 m ($\sigma_e \pm 0.23$ m). This expected NN separation is only 0.21 m larger than r_a, and the resulting R value is 0.98. R is therefore within the 2σ confidence limits of the Poisson model. Similarly, c has a value of −0.94 and is within its 2σ confidence limits. We therefore conclude that the distribution of NN distances in the Hnúta group is consistent with a Poisson distribution.

The Hnúta satellite (subdomain 1.1) differs from the previous two cases (i.e., complete study area and the Hnúta group) in that its r_a is 1.98 and thus lower than r_e. The resulting R and c values are outside their respective 2σ confidence limits, and so the Poisson model is rejected. Since R exceeds the upper 2σ confidence limit, we conclude that rootless eruption sites in subdomain 1.1 exhibit a statistically significant repelling relative to the Poisson model.

The Hrossatungur group, including domains 3–6, has a c value exceeding its 2σ limits and an R value outside its lower 2σ limit. Rootless eruption sites in Hrossatungur group is therefore similar to the study area as a whole in that it exhibits a statistically significant clustering relative to the Poisson model.

To determine how the spatial distribution of rootless eruption sites varies with scale, we have examined four subdomains in Hrossatungur group. Each subdomain represents a geographically continuous portion of an independently formed domain with >30 rootless eruption sites (Hamilton et al. 2010). Subdomain 3.1 has an r_e value of 6.69 m ($\sigma_e \pm 0.46$ m), which is 1.26 m smaller than r_a. The resulting R value (1.19) is slightly above the ideal value of 1.06. The R and c values are thus within their respective 2σ limits, which indicates that the distribution of rootless eruption sites in subdomain 3.1 is consistent with a Poisson model. In subdomain 4.1, both R and c are within their respective 1σ limits, which implies greater consistency

Table 2 Measured NN properties of the input distributions

Input distribution properties	All	Hnúta group (domain 1)	Hnúta satellite (subdomain 1.1)	Hrossatungur (domains 3–6)	Subdomain 3.1	Subdomain 4.1	Subdomain 5.1	Subdomain 6.1
N (N_i)	2216 (2193)	777 (756)	111 (98)	1199 (1176)	65 (56)	65 (54)	38 (31)	130 (121)
A_{hull} (m^2)	1.27×10^6	4.30×10^5	2.97×10^4	4.57×10^5	9.96×10^3	3.85×10^3	3.18×10^3	6.49×10^3
ρ_i (N_i/A_{hull}) (m^2)	1.72×10^{-3}	1.76×10^{-3}	3.30×10^{-3}	2.57×10^{-3}	5.62×10^{-3}	1.40×10^{-2}	9.75×10^{-3}	1.86×10^{-2}
$r_a \pm 1\sigma_e$ (m)	8.67±0.11	11.71±0.22	10.68±0.39	6.52±0.11	7.95±0.40	4.82±0.28	6.72±0.45	4.44±0.15
Min. to max. NN distance (m)	0.02 to 38.00	0.42 to 38.00	0.09 to 20.10	0.02 to 33.82	3.01 to 18.14	2.55 to 12.43	2.57 to 11.86	1.63 to 9.19
Skewness[a]	1.49	1.11	−0.64	1.94	0.71	1.24	0.33	0.53
Kurtosis[a]	6.15	4.81	4.25	9.85	3.92	4.92	2.26	2.87

[a] Presented in the standardized form described by Baloga et al. (2007)

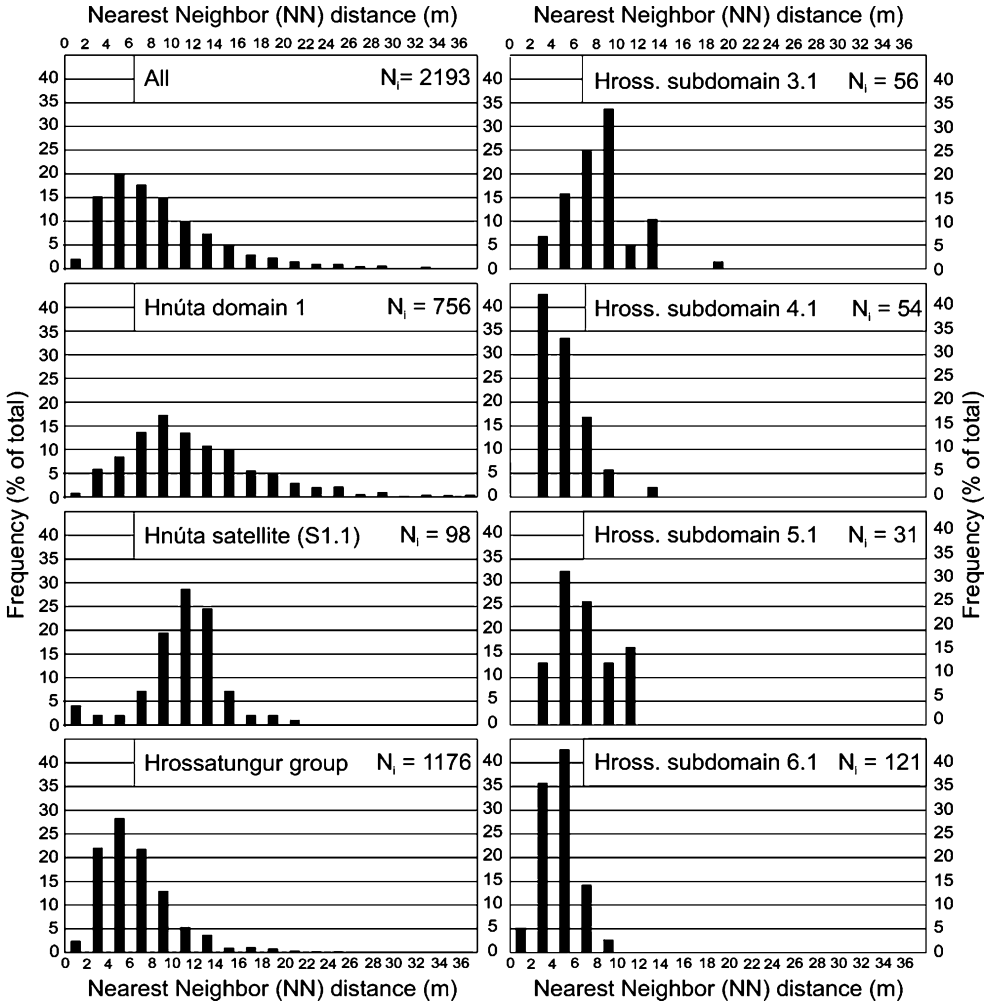

Fig. 3 Histograms of measured nearest neighbor (*NN*) distances (r_a)

with the Poisson model than fits that exceed 1σ, but remain within 2σ. Consequently, rootless eruption sites in subdomain 4.1 are strongly consistent with a Poisson NN distribution. Subdomain 5.1 has an R value within its 1σ limit of significance, but the Poisson model must be rejected because c is outside its 2σ limits. Subdomain 6.1 has an r_e value of 3.66 m (σ_e±0.17 m). The resulting c value (4.45) is outside its 2σ limit and R exceeds its upper 2σ limit, which implies that subdomain 6.1 has a statistically significant repelled distribution relative to the Poisson model.

Voronoi analyses

Analysis of NN distances provides information about pairwise interactions between rootless eruption sites in the study area, but it does not describe their spatial organization as an interconnected system. To examine how rootless eruption sites combine into a network, we have developed Voronoi tessellations defining the zone of maximum influence around each eruption site (Fig. 6). By comparing the mean area of measured Voronoi cells (v_a) to the optimum cell area (v_e) that would be expected if all NN distances had a uniform value of r_a (Eq. 4), we can determine if the input distribution tends toward a maximum packing arrangement. If V values, defined by the ratio of v_a to v_e, approach 1, we may conclude that the measured Voronoi cell areas are approaching the optimum area defined by initial environmental conditions and competition for limited resources.

Table 4 and Fig. 7 summarize the results of the Voronoi analyses. In the overall study region (labeled All) and the Hrossatungur group, v_a values are 507.69 m^2 (σ_e± 16.62 m^2) and 357.68 m^2 (σ_e±17.87 m^2), respectively. Values of V are 7.80 and 9.72. These departures of v_a from v_e suggest that rootless eruption sites in the complete study area and the Hrossatungur group do not exhibit an overall tendency to self-organize into arrangements that maximize the utilization of homogeneously distributed resources. This suggests the possibility that resources are heterogeneously distributed throughout the complete study area and the Hrossatungur group, which is consistent with the clustered NN distributions observed in these two zones.

Table 3 NN results relative to the Poisson model

Poisson NN model	All	Hnúta group (domain 1)	Hnúta satellite (subdomain 1.1)	Hrossatungur (domains 3–6)	Subdomain 3.1	Subdomain 4.1	Subdomain 5.1	Subdomain 6.1
$r_e \pm 1\sigma_e$ (m)	12.05±0.14	11.92±0.23	8.70±0.46	9.86±0.15	6.69±0.49	4.22±0.30	5.06±0.48	3.66±0.17
R (ideal R given N_i)	0.72 (1.01)	0.98 (1.02)	1.23 (1.04)	0.66 (1.01)	1.19 (1.06)	1.14 (1.06)	1.08 (1.33)	1.21 (1.04)
R thresholds at 1σ	1.00 and 1.03	1.00 and 1.04	0.98 and 1.10	1.00 and 1.03	0.98 and 1.15	0.98 and 1.15	0.97 and 1.19	1.09 and 1.15
R thresholds at 2σ	0.98 and 1.04	0.97 and 1.06	0.93 and 1.16	0.98 and 1.05	0.90 and 1.23	0.90 and 1.23	0.86 and 1.30	0.85 and 0.99
c (ideal c given N_i)	−25.14 (0.66)	−0.94 (0.77)	4.30 (0.86)	−22.24 (0.75)	2.76 (0.88)	0.88 (1.98)	3.48 (0.88)	4.45 (0.85)
c thresholds at 1σ	−0.50 and 1.83	−0.28 and 1.82	−0.23 and 1.94	−0.31 and 1.81	−0.28 and 2.04	−0.28 and 2.04	−0.29 and 2.06	−0.23 and 1.93
c thresholds at 2σ	−1.41 and 2.73	−1.33 and 2.86	−1.32 and 3.03	−1.33 and 2.83	−1.44 and 3.19	−1.44 and 3.20	−1.47 and 3.23	−1.31 and 3.01
Conclusions	Model rejected (>2σ limits of c)	Model supported (<2σ limits of c)	Model rejected (>2σ limits of c)	Model rejected (>2σ limits of c)	Model supported (<2σ limits of c)	Model supported (<1σ limits of c)	Model rejected (>2σ limits of c)	Model rejected (>2σ limits of c)
Implications	Clustered relative to model (>2σ limits of R)	The data fit the model (<2σ limits of R)	Repelled relative to the model (>2σ limits of R)	Clustered relative to model (>2σ limits of R)	The data fit the model (<2σ limits of R)	The data fit the model (<1σ limits of R)	The data do not fit the model (<1σ limits of R)	Repelled relative to the model (>2σ limits of R)

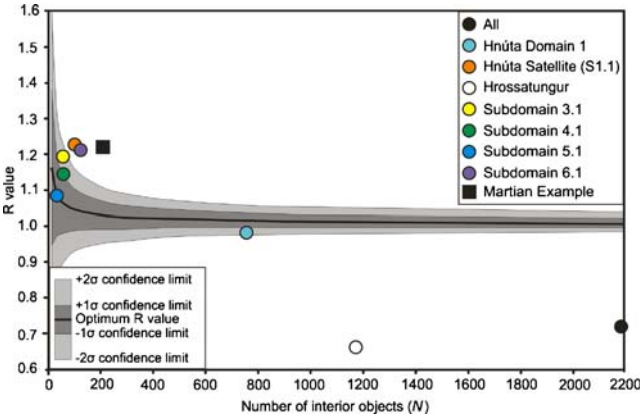

Fig. 4 Plot of R values for each region in the study area with sample-size-dependent thresholds of significance. The complete study area (All) and Hrossatungur group exhibit clustering relative to the Poisson (random) model (i.e., $R<-2\sigma$ threshold); domain 1 of the Hnúta group and Hrossatungur subdomains 3.1, 4.1, and 5.1 exhibit Poisson distributions; Hnúta satellite subdomain 1.1 and Hrossatungur subdomain 6.1 exhibit repelled distributions relative to the Poisson model (i.e., $R>+2\sigma$ threshold). The *black square* shows the results from a rootless cone group in eastern Elysium Planitia, Mars (after Baloga et al. 2007)

The Hnúta group (domain 1) has v_a equal to 529.37 m^2 (σ_e±16.70 m^2) and V equal to 4.46. This implies that interactions between neighboring rootless eruption sites did not result in a well-developed self-organization, which is consistent with the observed Poisson (random) NN distribution in domain 1.

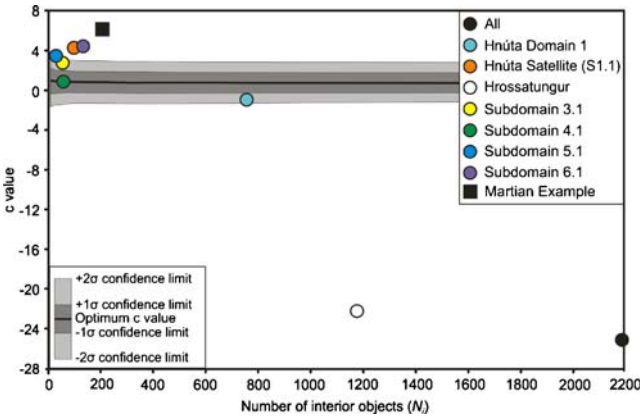

Fig. 5 Plot of c values for each region in the study area with sample-size-dependent thresholds of significance. These results confirm the statistical significance of the Possion (random) distributions, based on R value results, for the Hnúta group and Hrossatungur subdomains 3.1 and 4.1. The implication that Hrossatungur subdomain 5.1 has a Poisson distribution is rejected because its c value exceeds its sample-size-dependent threshold of significance at 2σ. The c values for the complete study area (All), Hrossatungur group, Hrossatungur subdomain 6.1, and Hnúta satellite (subdomain 1.1) all have R and c values outside their respective thresholds of significance and thus exhibit non-random spatial organizations. The *black square* corresponds to a rootless cone group in eastern Elysium Planitia, Mars (after Baloga et al. 2007)

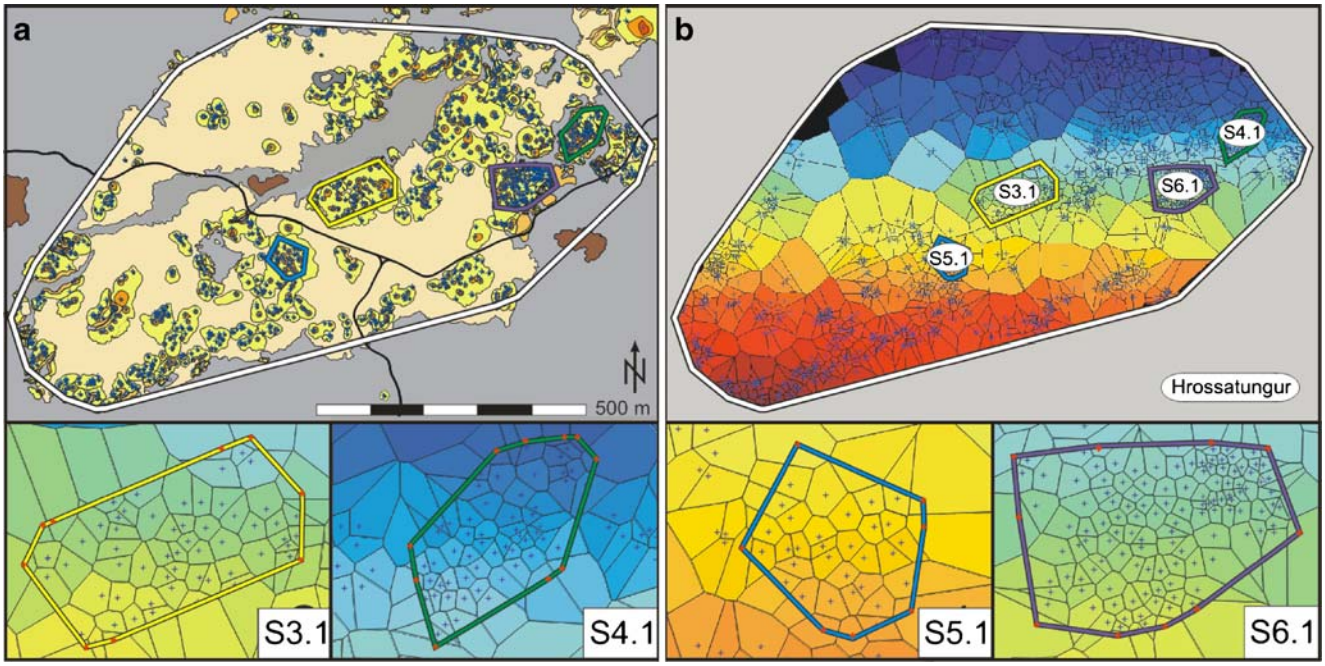

Fig. 6 **a** Locations of explosion sites (*crosses*) within the Hrossatungur group (bounded by a white convex hull) and its four constituent subdomains: S3.1 (*yellow*), S4.1 (*purple*), S5.1 (*cyan*), and S6.1 (*green*). **b** Voronoi tessellation of rootless eruption sites in the Hrossatungur group. Voronoi cell areas exhibit substantial variation throughout the Hrossatungur group as a whole, but in each of the contemporaneously emplaced subdomains, the Voronoi cells adopt a honeycomb-like arrangement of approximately equal cell area. *Colors* in **b** identify unique cells

The Hnúta satellite (subdomain 1.1) and Hrossatungur subdomains 3.1, 4.1, and 6.1 have V values of 2.68, 2.91, 2.32, and 2.62, respectively. Rootless eruption sites in these four regions generated tessellations of Voronoi cells that are within two to three times their optimum area. This suggests a tendency for rootless eruption sites to self-organize in order to maximize the region of influence around each explosion site and maximize resource utilization. This process is consistent with repelling observed in the NN distributions of Hnúta subdomain 1.1 and Hrossatungur subdomain 6.1. Subdomain 5.1 of the Hrossatungur group has v_a equal to 62.90 m^2 (σ_e±4.69 m^2) and V of 3.13, which suggests that relative to the other subdomains, subdomain 5.1 has a similar, but weaker, tendency toward developing a maximum packing arrangement.

Discussion

Scale-dependent controls on the spatial distribution of rootless eruption sites

The results of this study differ significantly from previous investigations which concluded that rootless eruption sites exhibit only clustered distributions (Bruno et al. 2004, 2006). On the scale of complete groups, we have demonstrated

Table 4 Voronoi results

Region	r_a (m)	Mean Voronoi cell area (v_a±1σ_e) (m^2)	Optimum Voronoi cell area (v_e) (m^2)	Difference (v_a − v_e) (m^2)	Ratio (V=v_a/v_e)
All	8.67	507.69±16.62	65.10	442.60	7.80
Hnúta group (domain 1)	11.71	529.37±16.70	118.75	410.62	4.46
Hnúta satellite (S1.1)	10.68	264.90±17.13	98.69	166.21	2.68
Hrossatungur (domains 3–6)	6.52	357.68±17.89	36.82	320.86	9.72
Subdomain 3.1	7.95	159.14±12.89	54.73	104.41	2.91
Subdomain 4.1	4.82	90.58±4.69	39.11	51.47	2.32
Subdomain 5.1	6.72	62.90±7.87	20.11	42.78	3.13
Subdomain 6.1	4.44	45.01±2.59	17.05	27.96	2.64

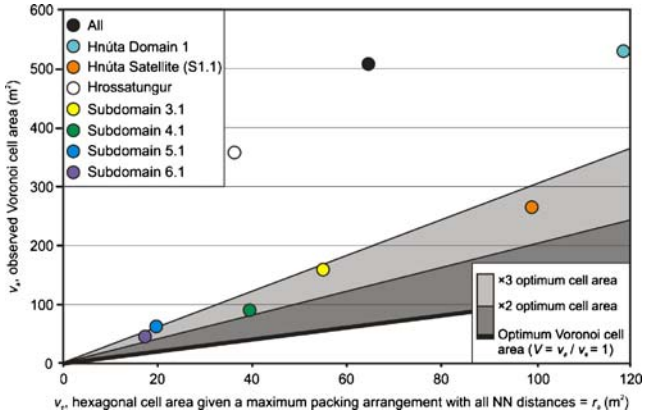

Fig. 7 Plot of mean measured Voronoi cell area (v_a) versus optimum Voronoi cell area (v_e) given a maximum packing arrangement with all of the rootless explosion sites in each region separated by the mean NN distance (r_a). The complete study area (All), Hnúta group, and Hrossatungur group do not show a tendency toward a maximum packing arrangement, whereas the Hnúta satellite subdomain 1.1 and Hrossatungur subdomains 3.1, 4.1, and 6.1 show a tendency toward self-organization with mean Voronoi cell areas that are within two to three times their optimum values

that rootless eruption sites exhibit statistically significant clustering, but within these groups, there are domains and subdomains that exhibit random to repelled NN distributions. These variations in geospatial organization demonstrate that developing valid statistical inferences from NN analyses requires the use of logical unit boundaries and that the geological context provided by our field observations helped in refining our understanding of where these logical boundaries occur within volcanic rootless cone groups.

In our NN analyses, the resolution of our input data remained constant, while the scale of the region under consideration changed based on the examination of natural subdivisions within the dataset. Using this approach, we interpret the observed scale-dependent patterns of spatial organization in the context of resource availability and depletion. On the scale of the complete study region, lava and water resources are heterogeneously concentrated. For instance, Hamilton et al. (2010) demonstrated that spaces between rootless cone domains are occupied by kipuka. This implies that during the initial phases of the Laki eruption, these kipuka were topographic highs that deflected the path of the Laki lava into topographic lows. Prior to the Laki eruption, the topographic depressions would have been favorable sites for accumulating water—thus making these environments ideal locations for initiating molten fuel—coolant interactions (MFCIs) involving lava and groundwater (Wohletz 2002). The spatial distribution of rootless eruption sites can therefore be used to infer information about pre-eruption topography, lava flow thicknesses, molten lava supply, and groundwater distributions.

The largest rootless cones in the study area are located within the Hnúta group, which coincides with the inferred location of a boggy region at the southern end of the Varmárdalur valley, near the foot of the Galti-Hrossatungur ridge (Hamilton et al. 2010). The Galti-Hrossatungur ridge impeded the southward advance of the Laki lava, which concentrated the lava flow into a network of gullies as the flow moved toward the ridge crest. Explosive lava–water interactions within the gullies constructed rootless cone domains that inverted the landscape and thereby affected the flow of later lavas. Consequently, we attribute the overall clustering of rootless cone eruption sites in the study area to the preferential occurrence of rootless eruptions within pre-eruption topographic lows because these regions were the most favorable locations for concentrating both water and lava resources.

Heterogeneous resource concentration may account for the first-order clustering of rootless cones within the study area, but within these clusters, rootless eruption sites either formed randomly (e.g., domain 1 of the Hnúta group and Hrossatungur subdomains 3.1 and 4.1) or exhibit evidence of self-organization into repelled distributions (e.g., Hnúta subdomain 1.1 and Hrossatungur subdomain 6.1). Random spatial distributions may be due to the absence of pairwise interactions between simultaneously active rootless eruption sites and/or random overprinting of rootless eruption sites that form at later times. For instance, Hamilton et al. (2010) show that domain 1 exhibits an evolutionary sequence from widely distributed rootless eruptions to a concentration of active explosion sites along preferred pathways. This implies that the rootless eruption sites in the Hnúta group were not all simultaneously active and that the observed random NN distribution was generated, in part, by random overprinting processes that may be related to the development of the lava distribution system with time (Glaze et al. 2005).

Hnúta subdomain 1.1 and Hrossatungur subdomain 6.1 are of particular interest because they exhibit statistically significant repelled distributions, which imply that rootless eruption sites in these regions interacted with one another to develop a greater than random NN spacing. This self-organization process is supported by the Voronoi tests which show these regions have Voronoi cells that are within two to three times the area expected given a maximum packing arrangement.

Repelled distributions could result from (1) reorganization in the location of active explosion sites due to NN interactions or (2) cessation, or non-initiation, of rootless eruption sites at unfavorable locations due to location-dependent resource availability. Although rootless eruption sites may excavate vertically into the substrate, river-cut cross-sections through the Thjórsárdalur rootless cone group in Iceland provide evidence that rootless eruption sites exhibit minimal lateral migration after their initiation. The interpretation that rootless eruption sites tend to occupy

horizontally fixed locations has also been proposed by Jaeger et al. (2007) based on the properties of rootless tephra deposits on the surface of some lava flows in Athabasca Valles, Mars. We therefore attribute repelling of rootless eruption sites to location-dependent productivity within a water-limited system where rootless eruptions with access to insufficient groundwater supplies will either fail to initiate or terminate before activity has ceased at neighboring localities. Tephra deposition from longer-lived rootless eruption sites may then bury the surface expression of inactive sites to generate a final repelled NN distribution. This conclusion suggests that the surface expression of rootless eruption sites can be overprinted by tephra dispersal; however, variations in the duration and intensity of rootless eruptions preclude the definition of a constant length scale for this overprinting process.

The Voronoi analysis shows that even when NN pairs show a random distribution (i.e., no interaction), the system may develop an overall self-organization due to the location of other members of the network. Domain 1 of the Hnúta group (V=4.46) is the only region in the study area that exhibits a random NN distribution and very large deviation from its optimum Voronoi cell area. This supports the conclusion that its eruption sites were not active at the same time and, therefore, did not simultaneously compete for resources as a single network. In the following section, we compare our study area to an analogous rootless cone group on Mars to show how competition for limited water resources in favorable environments can cause rootless cone networks to develop patterns of self-organization in different planetary environments.

Rootless cone analogs on Mars

Figure 8 shows part of the Tartarus Colles cone group located in eastern Elysium Planitia, Mars (25–27° N, 170–171° E). In Figs. 4 and 5, we have plotted the NN statistics for this Martian rootless cone example based on the results of Baloga

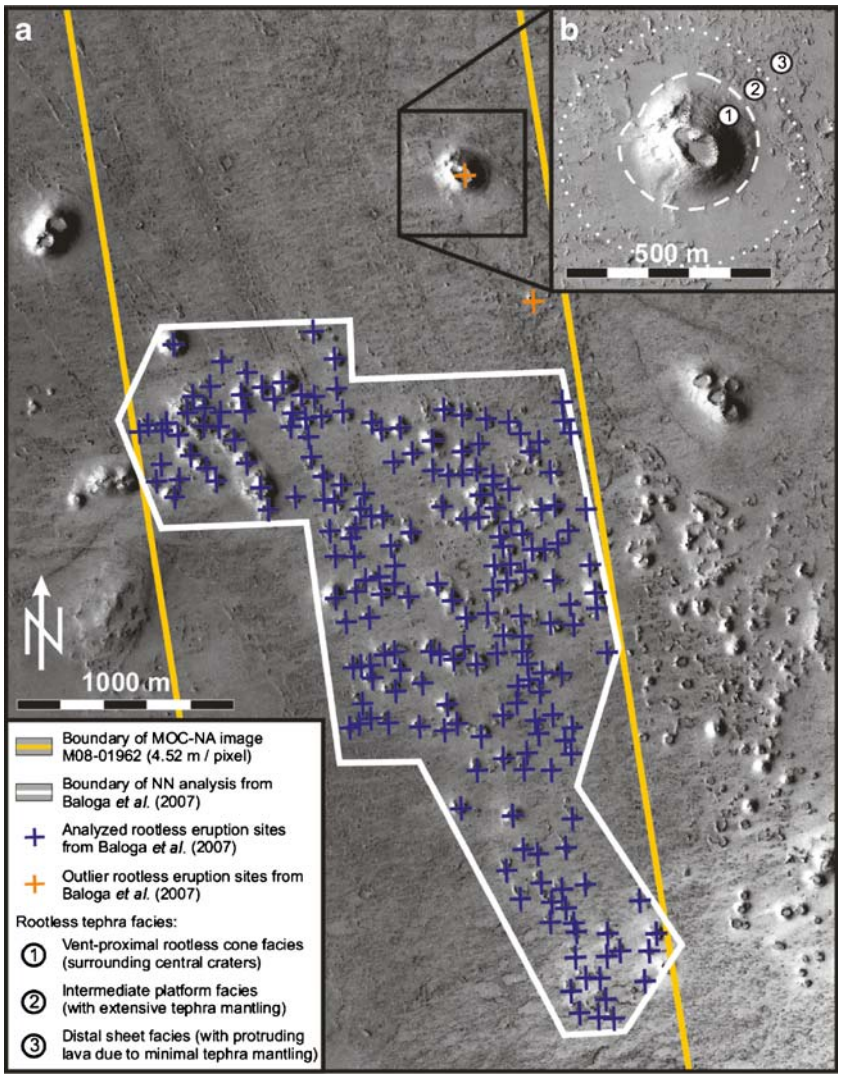

Fig. 8 Volcanic rootless cones within the Tartarus Colles cone group in eastern Elysium Planitia, Mars (25–27° N, 170–171° E). **a** A portion of Mars Reconnaissance Orbiter (*MRO*) Context Camera image (P02_001711_2055_XN_25N189W, 5.69 m/pixel, sub-solar azimuth (i.e., illumination direction measured clockwise from three o'clock) = 183.64°). This image shows the extent of the Mars Global Surveyor (*MGS*) Mars Obiter Camera (*MOC*) narrow angle (*NA*) examined by Baloga et al. (2007), the boundary of their feature field, rootless eruption sites analyzed in their study, and the outlier rootless eruption sites that were excluded from their NN analysis. The *inset* (**b**) shows part of MRO High-Resolution Imaging Science Experiment (*HiRISE*) image PSP_008528_2060 (0.25 m/pixel, sub-solar azimuth = 188.81°) which depicts the inferred boundaries between the vent-proximal ("1"), intermediate ("2"), and distal ("3") tephra facies with mantling of lava surface roughness that increases toward the central crater(s)

et al. (2007). Baloga et al. (2007) did not employ the convex hull method and were unable to delimit the complete extent of the feature field due to limited high-resolution satellite image availability. Nevertheless, their results exhibit intriguing similarities to the features observed within the Hnúta and Hrossatungur groups. In the Martian example, R and c values are 1.22 and 6.14, respectively. These R and c values are nearly identical to the repelled distributions in the Hnúta subdomain 1.1 (R=1.23, c=4.30) and Hrossatungur subdomain 6.1 (R=1.21, c=4.45), which suggests that the processes generating repelled eruption sites in our study area are similar to those in some regions on Mars.

The rootless cones in subdomain 6.1 and the Martian landforms depicted in Fig. 8 exhibit other striking similarities. For instance, the Martian landforms have repelled distributions (R=1.22, c=6.14), radial symmetry, and morphological facies associations that are typical of terrestrial rootless cones (Hamilton et al. 2010). These facies include vent-proximal cone deposits and an intermediate tephra platform that grades into a distal sheet deposit (Fig. 8b). The extent to which the platform and distal deposits mantle the underlying lava decreases with distance from source, which is evidenced by the increase in apparent roughness of the lava surface with greater distance from the central crater(s). Although aeolian modification may have reworked some of these tephra deposits—particularly within the unconsolidated platform and distal deposits—the common recurrence of these facies associations in the Tartarus Colles cone groups suggests that these landforms have inherited primary tephra emplacement structures that are analogous to terrestrial rootless tephra facies.

In the Hnúta and Hrossatungur groups, rootless cones with radial symmetry are typically produced by isolated rootless eruption sites that deposit tephra onto a stationary lava surface during short periods of explosive activity. In contrast, longer duration rootless eruptions tend to construct tephra complexes with interfingered tephra deposits that obscure the radial symmetry of individual cones. This observation supports the conclusion that the Martian landforms are rootless cones formed within a water-limited environment that was quickly depleted of mobile groundwater and thus could not form mature rootless tephra complexes with extensively interfingered deposits. The morphology of individual cones also provides evidence of a water-limited system in which initially energetic rootless explosions deposited tephra >250 m from source, evidenced by the masking of relief on the surface of the surrounding lava flows (e.g., Fig. 8b). Shadowing within the Martian rootless cone craters (Fig. 8b) suggests steep crater walls, which are inconsistent with the angle of repose for unconsolidated material but consistent with the late stage welded spatter deposits that are typical of water-limited rootless eruptions on Earth (Fagents and Thordarson 2007).

Interpretation

Self-organization during rootless eruptions

We hypothesize that the spatial organization of rootless eruption sites into repelled distributions on Earth and Mars reflects a balance between resource availability, depletion, and recharge within a network of active explosion sites. For instance, subdomain 6.1 of the Hrossatungur group provides excellent examples of statistically significant repelled distributions, which implies that longer-lived rootless eruption sites have self-organized into a configuration that maximizes the utilization of limited groundwater resources. Within this conceptual model, each rootless eruption site can be considered analogous to an extraction well into an aquifer (Fig. 9a). As lava comes into direct contact with the underlying groundwater, the water converts to steam and is removed from the aquifer during rootless explosions. This produces a cone of depression in the water table around the rootless eruption site. The Voronoi cell boundaries therefore approximate the surface projection of the zones of maximum interference between adjacent extraction wells.

In a hydrological system that contains multiple extraction wells, the drawdown in the hydraulic head at any point in a confined aquifer equals the algebraic sum of the drawdowns that would occur from each of the wells independently. Figure 9b illustrates a system that includes two extraction wells in an ideal aquifer with both wells pumping at the same rate (Q). If Q for each well is unequal, the symmetry about the plane AA^1 will be lost, but the principle of superposition will remain the same. For reasons discussed in Appendix 2, rigorous modeling of rootless eruptions as network of extraction wells is beyond the scope of this paper. However, the extraction well analog does offer a conceptual framework for understanding how the superposition of drawdown curves in the vicinity of rootless eruption sites can modify the availability of water in the surrounding aquifer and thus promote self-organization (Fig. 9c).

Resource competition and alternatives to Poisson NN distributions

In this study, some rootless eruption sites (i.e., Hnúta subdomain 1.1 and Hrossatungur subdomain 6.1) exhibit repelling relative to a Poisson model and yet are clustered with respect to the k=1 scavenged Poisson distributions (Appendix 1). Scavenged Poisson models are intended to describe a physical system in which resources that would

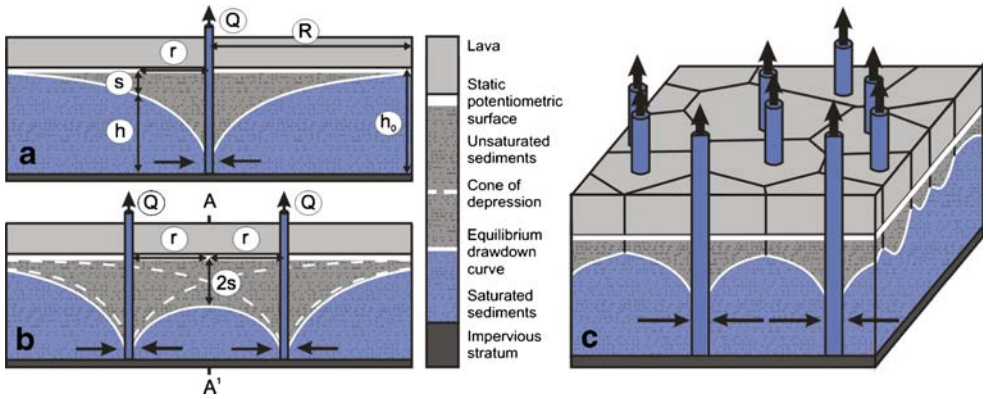

Fig. 9 **a** Diagram of the cone of depression produced by a fully penetrating extraction well within an aquifer, which in this case is initially confined. Q discharge, R maximum radius of influence, r radial distance from the extraction to an arbitrary point, h_0 constant initial hydraulic head; h equilibrium hydraulic head at r and time t, and s drawdown (i.e., $s = h_0 - h$) of the potentiometric surface at r and t. **b** Diagram of an aquifer system that includes two extraction wells, both of which are pumping at the same Q. Note that the drawdown in the water table produced by each extraction well sums linearly to define the net potentiometric surface, and consequently, at the midpoint between the two wells, the net drawdown will be $2s$. **c** A network of n extraction wells within an aquifer with the midpoints between each well being defined by the cell boundaries in a Voronoi tessellation

otherwise be used to form the kth nearest neighbor are consumed to create an annulus in which explosion sites are not expected to form (Baloga et al. 2007). As the order of k increases, the distance between NNs is expected to increase; however, the k=1 scavenged Poisson model over predicts the strength of resource scavenging process during rootless eruptions.

There are many reasons that could account for the failure of the scavenging process to describe the effects of resource competition during rootless eruptions. For instance, the scavenging NN models of Baloga et al. (2007) and Beggan and Hamilton (2010) are scale-free distributions in which modifications to expected NN distances depend upon the number of objects participating in the scavenging process and not on the location of the objects. This is an unrealistic condition for resource-scavenging phenomena in nature which have a fixed upper limit to their extent. Alternative resource consumption scenarios may therefore be more appropriate, but it should not be assumed that length scales for scavenging processes will be equal for all members of the distribution. Rootless eruptions vary in their duration, intensity, and volume of erupted material. This suggests that a meaningful scavenging radius would depend upon the volume of consumed resources and thus would not be constant for all rootless eruption sites. Poisson NN models assume azimuthal symmetry in terms of resource distributions, but this assumption could be violated if there were heterogeneities in groundwater abundance, substrate hydrology, preferred lava pathways, or topographic influences (n.b., we infer that topography exerts strong controls on rootless eruption site distributions within groups and domains, but not over the local scale of subdomains). Existing scavenging models are point processes which assume that objects can by simulated by points and resources will either be present or consumed at each of these localities. The hydrological model presented in Fig. 9 suggests that resource consumption is not a Boolean process, but rather that groundwater scavenging would continuously decrease with distance away from each rootless eruption site. Consequently, NN separations in subdomain 1.1 and Hrossatungur subdomain 6.1 might be better approximated by fractional scavenging processes with k between 0 and 1. Nonetheless, all Poisson NN distributions are derived under the assumption that initial conditions, influences, and formational mechanisms will result in a Poisson process (Baloga et al. 2007). This may not be a valid assumption for all geological systems and, as an alternative to Poisson models, Baloga et al. (2007) proposed the application of logistic curve fitting to NN distributions.

The relationship between the carrying capacity of an environment and its resources can be quantified using the logistic equation (Verhulst 1838; Lotka 1925) which has been used extensively in biology and ecology to model the growth of organisms and populations (Balakrishnan 1991). As a self-limiting logistic process, we would expect rootless eruptions to initiate where required resources (i.e., lava and groundwater) are present, but that increased rootless eruption duration and/or intensity would increase resource depletion. Thus, rootless tephra volumes would be proportional to resource abundance, but erupted rootless tephra volumes would be limited by competition with other rootless eruption sites that simultaneously consume resources in their vicinity. To maximize the use of limited resources, active rootless eruption sites would develop the repelled distribution with NN distances, reflecting a balance

between resource availability and the strength of the competition. Within Hnúta subdomain 1.1 and Hrossatungur subdomain 6.1, mean rootless eruption crater diameters are 10.5 m (σ=5.3 m, σ_e=0.5 m) and 4.1 m (σ=2.3 m, σ_e=0.4 m), respectively, and the corresponding r_a values are 10.7 m (σ=3.8 m, σ_e=0.4 m) and 4.4 m (σ=1.7 m, σ_e=0.2 m). Assuming that crater diameter can be used as a proxy for eruption duration and/or intensity, we would expect NN distances in subdomain 1.1 to be proportionally greater than those in subdomain 6.1, and this is precisely what is observed. Using Kolmogorov–Smirnov, Anderson–Darling, and chi-squared tests, NN distributions in Hnúta subdomain 1.1 and Hrossatungur subdomain 6.1 can be fit with logistic distributions, but we caution that these logistic fits can be misleading because there are other distributions that provide better fits to these data. Thus, while rootless eruption sites may appear to exhibit characteristics of self-limiting population growth, we conclude that previously proposed scavenging and logistic density distributions (Baloga et al. 2007) do not provide the best description of the underlying physical processes. Nevertheless, as more becomes known about explosive lava–water interaction systems, improved probability distribution models may be developed that build upon the hydrological considerations presented in "Self-organization during rootless eruptions" and Appendix 2.

Conclusions

By combining geospatial statistics with boundaries derived from field observations, we have quantified the spatial organization of rootless eruption sites in the Hnúta and Hrossatungur groups of the 1783–1784 Laki lava flow. On the scale of complete rootless cone groups, we have determined that rootless eruption sites cluster within pre-eruption topographic lows that concentrate both water and lava. Given an excess lava supply relative to groundwater in these favorable environments, rootless eruption sites may self-organize into repelled distributions that maximize the utilization of limited groundwater resources. This resource competition model can qualitatively explain observed patterns of spatial distribution among the rootless eruption sites of Hnúta and Hrossatungur groups, and it provides a framework for interpreting the paleo-environmental significance of rootless cone analogs on Mars. For instance, rootless cone analogs in eastern Elysium Planitia exhibit morphological and geospatial similarities to rootless cones in subdomain 6.1 of the Hrossatungur group. In both environments, spatter-dominated rootless cones with well-preserved radial symmetry and a repelled NN distribution imply that sheet lobe-fed rootless eruptions occurred within a water-limited system that quickly exhausted local groundwater supplies.

Our study therefore shows how statistical NN analyses can be combined with field observations and remote sensing to obtain information about self-organization processes within geological systems and the effects of environmental resource limitation on the spatial distribution of volcanic landforms. NN analyses may also be used to quantitatively compare the spatial distribution of landforms in different planetary environments and for supplying non-morphological evidence to discriminate between feature identities and geological formation processes.

Acknowledgments We thank Karen Pascal for her assistance in the field; Samuel Hulme and Ciarán Beggan for their assistance with GMT and MATLAB, respectively; Steve Baloga and Barbara Bruno for discussions relating to NN analysis; Benjamin Brooks and the Pacific GPS facility for providing DGPS survey equipment and post-processing resources; Bruce Houghton and Scott Rowland for their comments and suggestions during the preparation of this manuscript; Laszlo Keszthelyi and Lori Glaze for their thoughtful and thorough reviews; and financial support from the National Aeronautics and Space Administration (NASA) Mars Fundamental Research Program (MFRP) grant NNG05GM08G, NASA Mars Data Analysis Program (MDAP) grant NNG05GQ39G, Geological Society of America (GSA), and Icelandic Centre for Research (RANNÍS). SOEST publication number 1800. HIGP publication number 7806.

References

Allen CC (1979) Volcano–ice interactions on Mars. J Geophys Res 84:8048–8059

Balakrishnan N (1991) Handbook of the logistic distribution. Marcel Dekker, New York

Baloga SM, Glaze LS, Bruno BC (2007) Nearest-neighbor analysis of small features on Mars: applications to tumuli and rootless cones. J Geophys Res 112:E03002. doi:10.1029/2005JE002652

Beggan C, Hamilton CW (2009) New image processing software for analyzing object size-frequency distribution, geometry, orientation, and spatial distribution. Comput Geosci. doi:10.1016/j.cageo.2009.09.003

Bruno BC, Fagents SA, Thordarson T, Baloga SM, Pilger E (2004) Clustering within rootless cone groups on Iceland and Mars: effect of nonrandom processes. J Geophys Res 109:E07009. doi:10.1029/2004JE002273

Bruno BC, Fagents SA, Hamilton CW, Burr DM, Baloga SM (2006) Identification of volcanic rootless cones, ice mounds, and impact craters on Earth and Mars: using spatial distribution as a remote sensing tool. J Geophys Res 111:E06017. doi:10.1029/2005JE002510

Clark PJ, Evans FC (1954) Distance to nearest neighbor as a measure of spatial relationships in populations. Ecology 35:445–453

Fagents SA, Thordarson T (2007) Rootless volcanic cones in Iceland and on Mars. In: Chapman MG (ed) The geology of Mars: evidence from earth-based analogs. Cambridge University Press, Cambridge, pp 151–177

Fagents SA, Lanagan P, Greeley R (2002) Rootless cones on Mars: a consequence of lava–ground ice interaction. In: Smellie JL, Chapman MG (eds) Volcano–ice interaction on Earth and Mars. Geol Soc Lond Spec Publ 202:295–317

Frey H, Jarosewich M (1982) Subkilometer Martian volcanoes: properties and possible terrestrial analogs. J Geophys Res 87:9867–9879

Frey H, Lowry BL, Chase SA (1979) Pseudocraters on Mars. J Geophys Res 84:8075–8086

Glaze LS, Anderson SW, Stofan ER, Smrekar SE (2005) Statistical distribution of tumuli on pahoehoe flow surfaces: analysis of examples in Hawaii and Iceland and potential applications to lava flows on Mars. J Geophys Res 110:B08202. doi:10.1029/2004JB003564

Graham R (1972) An efficient algorithm for determining the convex hull of a finite planar point set. Inf Proc Lett 1:132–133

Greeley R, Fagents SA (2001) Icelandic pseudocraters as analogs to some volcanic cones on Mars. J Geophys Res 106:20527–20546

Hamilton CW, Fagents SA, Thordarson T (2007) Rootless cone archetypes and their relation to lava flow emplacement processes. Abstracts of the 2nd Volcano–Ice Interaction on Earth and Mars Conference, University of British Columbia, Vancouver, 19–22 June 2007

Hamilton CW, Thordarson T, Fagents SA (2010) Explosive lava–water interactions I: architecture and emplacement chronology of volcanic rootless cone groups in the 1783–1784 Laki lava flow, Iceland. Bull Volcanol. doi:10.1007/s00445-009-0330-6

Head JW, Wilson L (2002) Mars: a review and synthesis of general environments and geological settings of magma/H_2O interactions. In: Smellie JL, Chapman MG (eds) Volcano–ice interaction on Earth and Mars. Geol Soc Lond Spec Publ 202:27–57

Jaeger WL, Keszthelyi LP, McEwen AS, Dundas CM, Russell PS (2007) Athabasca Valles, Mars: a lava-draped channel system. Science 317:1709–1711. doi:10.1126/science.1143315

Jaeger WL, Keszthelyi LP, McEwen AS, Dundas CM, Russell PS (2008a) Response to comment on "Athabasca Valles, Mars: a lava-draped channel system". Science 320:1588c. doi:10.1126/science.1155124

Jaeger WL, Keszthelyi LP, McEwen AS, Milazzo MP (2008b) Phreatovolcanism in a deflating sheet flow: insights from HiRISE images of Athabasca Valles, Mars. International Association of Volcanology and Chemistry of the Earth's Interior, General Assembly, Reykjavík, 17–22 August 2008

Lanagan PD, McEwen AS, Keszthelyi LP, Thordarson T (2001) Rootless cones on Mars indicating the presence of shallow equatorial ground ice in recent times. Geophys Res Lett 28:2365–2367

Lotka AJ (1925) Elements of physical biology. Williams and Wilkins, Baltimore

Steingrímsson J (1788) Fulkomid Skrif um Sídueld. Safn til Sögu Íslands IV:58–69

Thorarinsson S (1951) Laxargljufur and Laxarhraun: a tephrachronological study. Geograf Annal H1(2):1–89

Thorarinsson S (1953) The crater groups in Iceland. Bull Volcanol 14:3–44

Thordarson T (2003a) The 1783–1785 A.D. Laki-Grímsvötn eruptions I: a critical look at the contemporary chronicles. Jökull 53:1–10

Thordarson T (2003b) The 1783–1785 A.D. Laki-Grímsvötn eruptions II: appraisal based on contemporary accounts. Jökull 53:11–47

Thordarson T, Self S (1993) The Laki (Skaftar Fires) and Grimsvotn eruptions in 1783–85. Bull Volcanol 55:233–263

Thordarson T, Self S, Oskarsson N, Hulsebosch T (1996) Sulfur, chlorine, and fluorine degassing and atmospheric loading by the 1783–1784 AD Laki (Skaftár Fires) eruption in Iceland. Bull Volcanol 58:205–225

Verhulst V (1838) Notice sur la loi que la population suit dans son accrossement. Corr Math Phys 10:113–121

Wohletz K (2002) Water/magma interaction: some theory and experiments on peperite formation. J Volcanol Geotherm Res 114:19–35